Biosensors and Bioelectronics 131 (2019) 149–155

Contents lists available at ScienceDirect

Biosensors and Bioelectronics

journal homepage: www.elsevier.com/locate/bios

Label-free electrochemical DNA biosensor for zika virus identification

Henrique Antonio Mendonça Faria[1], Valtencir Zucolotto[*,1]

Nanomedicine and Nanotoxicology Group, Physics Institute of São Carlos, University of São Paulo, CP 369, 13560-970 São Carlos, SP, Brazil

ARTICLE INFO

Keywords:
DNA biosensor
Thermal evaporation
Label-free
Diagnosis
Zika virus
Dengue virus

ABSTRACT

Seventy years after its discovery, the zika virus emerged in Brazil and spread rapidly throughout the Americas, bringing unusual complications such as microcephaly. The World Health Organization classifies zika as the most harmful viral disease today and considers the development of new diagnostic methods for zika and related diseases, such as dengue, urgent. Although there are tests to identify both infections, current diagnostic methods are slow, nonspecific, and costly. This study describes an impedimetric electrochemical DNA biosensor for label-free detection of zika virus. Disposable electrodes were fabricated by thermal evaporation on polyethylene terephthalate substrates covered with a nanometric gold layer manufactured in three-contact configurations. The disposable, evaporated electrodes were morphologically characterized by atomic force microscopy and scanning electron microscopy. The electrode surface was characterized by electroanalytical techniques. Genetic sequences of primers and complementary capture probes were designed based on analysis of the zika and dengue virus genomes. The biosensor used a three-contact electrode to identify DNA sequences in a drop of sample, and for detection of zika virus sequences, it allowed for direct reading of the hybridization event without labeling on disposable electrodes and with a 1.5 h response time. In this system, impedance measurements indicated a limit of detection of 25.0 ± 1.7 nM. The developed biosensors showed selectivity for zika in the synthetic DNA assays, and therefore, are promising for clinical analysis.

1. Introduction

The zika virus is a flavivirus of the *Flaviridae* family of the same genus as the viruses that cause dengue and yellow fever. The zika virus remained in obscurity for 70 years, and as of March 2015 no case had been reported in South America (Petersen et al., 2016). It was then introduced into Brazil from the Pacific islands and, within a year, spread rapidly throughout the Americas (Fauci and Morens, 2016). The emergence of the zika epidemic in Brazil in 2015 left the world on alert because it was accompanied with aggravating factors such as microcephaly and sexual transmission, factors that were not previously observed to be involved in flaviviruses. The coexistence of zika and dengue infections is evidence for the need for development of more efficient low cost diagnostic methods that can identify and differentiate these two diseases. Infections of the zika virus in the Americas are still difficult to assess clinically because at the onset, symptoms are nonspecific and the cross-reactivity of antibodies to other flaviviruses such as dengue and yellow fever complicates the serological diagnosis. Therefore, given the history of high incidence of dengue in the region, millions of zika infections are going undiagnosed and the virus continue to spread (Bhatt et al., 2013; Musso et al., 2015). According to the World Health Organization (WHO), there is an urgent need to produce and develop new diagnostic methods to identify zika virus related infectious diseases (Haug et al., 2016).

There are three main diagnostic methods currently used for zika virus detection: viral isolation, serological identification, and molecular analyses (Yang and Narayan, 2017). The viral isolation technique involves the incubation of cell cultures, requiring a couple of days of incubation, being not efficient in the clinical setting. Serological identification based on antigens/antibodies interactions, on the other hand, may exhibit reduced specificity due to cross-reaction with others flaviviruses. Finally, the molecular analysis, using tools such as reverse transcription polymerase chain reaction (RT–PCR) and real-time PCR, differentiates between the zika virus and other species, such as dengue fever and yellow fever. Since its development, PCR has become a major tool for viral characterization.

Alternative techniques have been developed for RNA amplification (Singh et al., 2018). Among them, nucleic acid sequence based amplification (NASBA) consists of continuous isothermal amplification of nucleic acids in a single solution (Compton, 1991). Based upon this technique, a molecular-based diagnostics method composed of paper-based colorimetric detection and NASBA-based RNA amplification was

* Corresponding author.
E-mail addresses: henrique.fisica@ifsc.usp.br (H.A.M. Faria), zuco@ifsc.usp.br (V. Zucolotto).
[1] Authors contributed equally to the paper.

https://doi.org/10.1016/j.bios.2019.02.018
Received 18 December 2018; Received in revised form 31 January 2019; Accepted 12 February 2019
Available online 19 February 2019
0956-5663/

proposed for the molecular analysis of the zika virus (Pardee et al., 2016). This detection approach can reduce the total time of diagnosis, including sample collection, RNA extraction, RNA amplification, and colorimetric detection to 3 h.

Real-time loop-mediated isothermal amplification (RT-LAMP), another isothermal method (Notomi et al., 2000), was used for rapid detection of the zika virus as reported by Song et al. (2017). This low-cost and sensitive platform is composed by a disposable cassette that executes all operations from sample introduction to detection. The chemically-heated cup is coupled with a smartphone device, which is used as a flashlight to excite the fluorescent dye, as well as to analyze the images and estimate the virus concentrations. The developed platform can detect the zika virus in oral samples in less than 40 min (Song et al., 2017). In another study, Ganguli et al. developed a microfluidic platform for the simultaneous detection of zika, chikungunya, and dengue virus in the differentiation stages from whole blood samples using the same type of colorimetric detection with a smartphone (Ganguli et al., 2017).

Biosensors are advantageous in relation to other (Polymerase Chain Reaction) PCR product analysis techniques because they can add speed and precision to the molecular assay and can also perform simultaneous analysis of multiple analytes (Janegitz et al., 2014). An electrochemical DNA biosensor is defined by the International Union of Pure and Applied Chemistry (IUPAC) as a biosensor composed of a DNA and an electrochemical signal transducer (Labuda et al., 2010). DNA biosensors are based on the event of hybridization, which, in molecular biology, consists of hydrogen bonding between bases of a capture tape immobilized on the biosensor and a target ribbon present in the sample. DNA biosensors can be divided into two major groups, labeled and free (Ozsoz, 2012). In labeled biosensors, one of the approaches is based on the electrochemical response of an active redox marker that changes its concentration upon DNA hybridization. The markers are called hybridization indicators and have high affinity for ssDNA or dsDNA. The most common are complex metals and dyes that interact with the hydrogen bonds of dsDNA or have binding selectivity to the triple H-bonded bases guanine and cytosine.

Label-free genosensors have a great advantage for detecting genetic material in forensic medicine and clinical analyses, since they simplify the steps required for detection. Direct detection eliminates the marking steps, reducing the time and cost of analysis. Thus, label-free detection is advantageous and allows for the application of genosensors in diagnosis. During label-free detection, hybridization causes changes in the electrical properties of the electrode surface such as impedance, resistance (Li et al., 2005), and potential (Ingebrandt et al., 2007) that can be measured as an analytical signal. One of the most commonly used techniques in label-free genosensors is Electrochemical Impedance Spectroscopy (EIS) (Chang and Park, 2010; Gebala and Schuhmann, 2012). The interest in EIS can also be attributed to the possibility of collecting spectra over a wide range of frequencies, allowing the complete characterization of the surface in a short time interval (Lisdat and Schaefer, 2008). In EIS measurements, the hybridization of the complementary tape with the immobilized capture tape is detected by the variation of the load transfer resistance (Rct), taken from the impedance spectrum (Nyquist plot). Efforts to combine EIS with DNA detection focus on increasing sensitivity by means of immobilization methods (Park et al., 2008) capture sequence type (Keighley et al., 2008), and surface coverage (Witte and Lisdat, 2011) such as the use of different materials in the functionalization of the surface of the transducer (Chen et al., 2009).

Regarding the platform for construction of label-free biosensors, the use of disposable electrodes is of great interest because the regeneration of electrodes is not desirable for diagnostic purposes. The method for making disposable electrodes requires the thermal evaporation of thin films in a vacuum chamber (Golan et al., 1992). In this type of manufacturing, also called metallization, vapor-like particles solidify on the target substrate. The evaporation provides a homogeneous metal surface, of low roughness and free of pollutants when compared to the screen-printed process. In addition, the evaporation process is extremely reproducible and involves a reduced number of steps, materials, and solvents, which is advantageous to the production sector.

The use of gold electrodes for anchoring capture DNA probes is frequently adopted in DNA biosensors. On gold electrodes, the capture sequences are immobilized by covalent attachment at the thiol modification (-R-SH) (Watterson et al., 2002; Oliveira et al., 2014). This is a stable bond that enables single-point attachment of the platform preserving the conformational mobility of the DNA strand. Covalent immobilization is advantageous because electrostatic bonds from other parts of the backbone skeleton to the surface are unstable and may induce loss of specificity in hybridization (Gooding and Darwish, 2012). In addition to DNA, mercaptohexanol (MCH) was used as an intercalator to block the sites not occupied by the ligated DNA and favor only the complementary bonds between the sequences. The functionalization of the electrode surface with DNA or DNA-intercalators is called self-assembling monolayers (SAMs), which is widely used in DNA biosensors. In a study by Papadopoulou (Papadopoulou et al., 2015) the identification of *Yersinia Pestis* polymorphism with 262 bases amplicon polymerase chain reaction (PCR) was performed in the unpurified form. A careful methodology for extraction and amplification in an asymmetric duplex PCR was developed. An electrochemical biosensor for pathogen detection by PCR amplicon analysis was recently presented by Yan et al. (2016). This study demonstrated that it is possible to apply the concept of direct detection, without the need for labeling with fluorophores to analyze a PCR amplicon.

In addition to the technologies cited above, electrochemical biosensors can represent alternative time-reducing molecular analysis methods for the zika virus. DNA biosensors can possibly replace detection by gel electrophoresis in PCR technology and be used after isothermal amplification techniques, such as NASBA and RT-LAMP. In this paper we report the development of a disposable, three-contact biosensor on a single test strip to perform the label-free detection of viral DNA sequences in one sample drop capable of analyzing sequences of the zika virus.

2. Experimental section

2.1. Materials and reagents

All reagents were of analytical grade and used as received. All aqueous solutions were prepared using ultrapure water purified with Milli-Q Millipore system (resistivity = 18.2 MΩ cm). Methanol and acetone were purchased from Synth. Tris(hydroxymethyl)aminomethane was purchased from Hexapur Bio Lab. DL-Dithiothreitol (DTT), potassium ferricyanide ($K_3[Fe(CN)_6]$), potassium ferrocyanide ($K_4[Fe(CN)_6]$), potassium hydroxide (KOH), sulfuric acid (H_2SO_4), potassium chloride (KCl), hydrogen chloride (HCl), sodium hydroxide (NaOH), sodium phosphate dibasic anhydrous (Na_2HPO_4), sodium phosphate monobasic dihydrate ($NaH_2PO_4{\cdot}2H_2O$), ethylenediaminetetraacetic acid (EDTA), and sodium chloride (NaCl) were purchased from Sigma-Aldrich.

Polyethylene terephthalate (PET) substrate sheets (30 × 30 cm, thickness of 1.0 mm) were purchased from Goodfellow (UK), gold (purity of 99.9%) was purchased from Marsan (Brazil), and Sephadex™ NAP™-5 column was purchased from GE Healthcare (UK).

TE buffer (10 mM) was prepared by mixing the stock solutions of 10 mM Tris and 0.10 mM EDTA. Phosphate buffer solution (PB, 0.20 M, pH 8.0) was prepared by mixing 0.20 M $NaH_2PO_4{\cdot}2H_2O$ and 50 mM Na_2HPO_4. Phosphate buffer saline solution (PBS, 0.20 M, pH 7.4) was prepared by mixing 0.20 M $NaH_2PO_4{\cdot}2H_2O$, 50 mM Na_2HPO_4, and 3,0 M NaCl.

2.2. Gold sensing platform fabrication

The electrochemical-sensing platform was planar three-electrode disposable strips. The gold working, auxiliary and reference electrodes were fabricated on a polyethylene terephthalate (PET) substrate. PET substrates (8.0 × 32 × 1.0 mm) were cleaned with methanol in an ultrasonic bath for 5 min, dried in N_2 flow, and then fixed in aluminum masks for evaporation. Thin gold film (150 nm) was deposited directly on PET using the sputtering technique in a BAK 750 Balzers chamber. The working electrode area was 3.8 mm^2 and the reaction area was 42.2 mm^2, accommodating 5 and 60 µL aqueous samples, respectively. The polyvinyl chloride (PVC) insulator layer Imprimax® (Brazil) was fixed with an acrylic adhesive after pretreatment of the gold surface. The cost of each electrode was estimated at $2.49, and the final product resulted in a uniform gold layer featuring high-reproduction that allows scale-up fabrication. AFM was employed to evaluate the morphology of the gold-PET electrodes by using a NanoSurf Flexa atomic force microscope (Nanosurf, Switzerland), in tapping mode, with a resonant frequency of 300 kHz and a vibration amplitude of 40.2 mV. The images were recorded in air under humidity control. Gwyddion software was used for image treatment.

2.3. DNA sequences

Primers and capture probe DNA were selected within the sequence of the gene encoding the NS5 nonstructural proteins by *Flavivirus* with genotypes lineage of the zika virus (East African), GenBank access NC_012532.1. Dengue virus serotype 1, NC_001477.1, was used as a non-complementary target sequence. An alignment with Clustal X software (Thompson et al., 1997) was carried out for the NS5 protein encoded region for zika and dengue virus. Forward and reverse primers were designed to be 24 and 23 bp (base pairs) long, with a melting temperature (T_m) of 65.3 °C and 69.4 °C, respectively. For primer design, Invitrogen PrimerQuest® Tool was used to analyze new primers that were selected to obtain the amplification of a 100 bp sequence located within NS5. The capture probe sequences are the same for the forward primer, but it is functionalized with a thiol group at the 5' and complementary to the 3' end of the target sequence.

2.4. Electrochemical measurements

All experiments were carried out at 25 °C after a drop casting of 60 µL of 0.1 M PB buffer containing the redox coupler $[Fe(CN)_6]^{3-/4-}$ at equimolar 5.0 mM in PB 0.1 M, pH 7.4, on the sensing area of gold-PET. The measurements were performed using a three-gold electrode strip connected to an Autolab PGSTAT 302 potentiostat galvanostat. Data acquisition and processing were performed using the OriginPro8G (OriginLab, USA). Cyclic voltammetry (CV) was used in the electrochemical characterization of the electrodes. The voltammograms, scanning range of –0.4 to + 0.4 V, were managed by GPES (general purpose electrochemical system) software, version 4.9. Differential pulse voltammetry (DPV) measurements parameters were: modulation time of 0.055 s, time interval of 0.0175 s, potential step of 5 mV, amplitude of modulation of 70 mV, and a scanning range of - 0.4 to + 0.4 V. Electrochemical impedance spectroscopy (EIS) measurements were performed with an AC perturbation with an amplitude of typically 5 mV_{pp}. The AC modulation frequency was swept down from 30 kHz to 0.1 kHz with 10 measuring points per decade in logarithmic distribution. EIS spectra were recorded using a FRA (frequency response analyzer).

2.5. Pretreatment of the gold electrode surface

A pretreatment procedure (Gebala and Schuhmann, 2010) was applied to the gold electrode prior to the DNA probe immobilization. Electrochemical polishing was performed using a three-electrode configuration consisting of an Ag/AgCl (in 3.0 M KCl) reference electrode, a platinum-spiral auxiliary electrode, and gold-PET as a working electrode. The three contacts of gold-PET electrode were connected together and electrochemically polished by cyclic voltammetry in 0.5 M H_2SO_4, first between 0 and + 1.8 V (vs Ag/AgCl) with a scan rate 0.5 V s^{-1} (30 scans) and then between 0 and + 1.6 V (vs Ag/AgCl) with a scan rate of 0.1 V s^{-1} (10 scans). The roughness factor of the electrodes was determined from the ratio of the electroactive area (A_{ea}) to the geometric area (A_{ge}) of the electrode (Hoogvliet et al., 2000). Briefly, the lateral contacts on gold-PET were isolated and the central electrode was used as a working electrode. A_{ea} was obtained from the integration of the gold oxide reduction peak charge (Q_{ox}), less the capacitive layer charge (Q_{dc}), and dividing by 360 µC cm^{-2}. A_{ge} was calculated from the diameter (2.2 mm) of the electrode surface (A_{ge} = 0.038 cm^2).

2.6. Pretreatment of thiol-probe DNA oligonucleotides

Synthetic DNA oligonucleotides, purified with high performance liquid chromatography (HPLC), were obtained lyophilized from Sigma-Aldrich. The thiol-probe oligonucleotides were treated with DTT to cleave the disulfide bonds of oligo dimers (Patolsky et al., 2001). The lyophilized oligonucleotides were dissolved in a 0.17 M PB solution (pH 8) containing 0.04 M of DTT. The reaction was allowed to proceed for 16 h at 25 °C room temperature. The thiol-probe DNA was then purified by elution through a Sephadex™ NAP™-5 column with 0.5 mL of 0.17 M PBS (pH 7.4). Purified SH-probe DNA stock solutions (1.2 µM) were prepared in the same elution buffer and used the same day in the electrodes.

2.7. SH-probe DNA oligonucleotide immobilization

The SH-probe DNA was immobilized onto the gold surface of a central electrode by dropping 5 µL of the 0.40 µM DNA solution and 0.17 M PBS (pH 7.4). The electrodes were incubated for 5 h at 45 °C in a humidified atmosphere chamber to prevent evaporation of the solution. After the chemisorption process, the electrodes were thoroughly rinsed with ultrapure water to remove any loosely bound capture strands.

2.8. DNA hybridization

Hybridization of probe-modified gold electrodes was carried out by placing a 5 µL droplet of target complementary and non-complementary DNA in 0.05 M phosphate buffer containing 0.20 M NaCl (pH 7.4) onto the modified central contact electrode surface. Prior to hybridization, the target DNA solution was heated to 95 °C for 5 min and rapidly cooled in an ice bath. The formation of the double helix with the capture DNA immobilized on the biosensor is facilitated by target DNA denaturation, i.e., the heating procedure opens any hairpin leads. Furthermore, upon cooling, the sequence is kept rectilinear and free of new bonds until the hybridization event occurs. Hybridization was carried out for 1.5 h at 25 °C in a humidified atmosphere chamber to prevent evaporation of the solution. Afterwards, the electrode was rinsed with ultrapure water, dried under N_2, and the electrochemical measurements were carried out at a temperature of 25 °C in a drop of 60 µL, with Supporting electrolyte $[Fe(CN)_6]^{3-/4-}$ 5.0 mM in PB 0.1 M, pH 7.4.

3. Results and discussion

3.1. Morphological and electrochemical characteristics of the gold sensing platform

The formation of self-assembled monolayers (SAMs) is directly influenced by surface roughness (R). High values for R hinder the orientation of the monolayers, since sites not filled with thiol-DNA are exposed favoring the passage of electric charges. The roughness of the

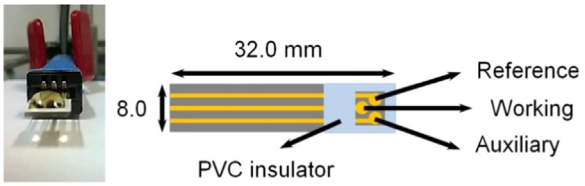

Fig. 1. Gold-PET electrode. Droplet of 60 µL of the electrolyte and biosensor contacts: central contact, working electrode and side contacts as reference and auxiliary electrode.

gold-PET electrodes was compared, to electrodes made from typical materials, such as glass and mica using atomic force microscopy. Fig. S-1 shows the roughness profile was taken from the AFM topography images of the PET substrate and the surface evaporated with Au. The surface roughness (R_a) and mean square roughness (R_{rms}) of the PET substrate evaporated with gold, shown in Table S-1, were compared with the roughness of the glass and mica evaporated simultaneously in the same chamber. The X-Ray Energy Dispersive Spectroscopy (EDS) spectrum analysis of the surface of the gold-PET substrate, Fig. S-2, reveals significant absence of other metallic elements. The morphological analysis showed that the conductive surface has a roughness close to other surfaces, such as glass and mica, which is a favorable feature for the formation of self-assembled monolayers.

For characterizations outside the electrochemical cell, the gold-PET electrode was connected to the Autolab potentiostat galvanostat through three-contact terminals, as shown in Fig. 1. The voltammetry measurements were performed in a drop of 60 µL in the reaction region, with the central contact acting as a working electrode and the two lateral electrodes acting as reference and auxiliary electrodes.

The cyclic voltammograms of the gold-PET evaporated electrodes with 10–400 mV s^{-1} scan rates, as shown in Fig. S-4. The anode current density (J_{pa}) is linearly dependent on the square root of the sweep velocity. The reversibility parameters, in 100 mV s^{-1}, were: ΔE_p = (97.0 ± 10.0) V and $| I_{pa} / I_{pc} |$ = (1.04 ± 0.20).

3.2. Design of primers, capture probes and target sequences for the detection of zika viruses

Details concerning primer, probes, and target synthetic oligonucleotides were listed in Table S-2 and identified as follows: **Zika virus**: Zfor- primer forward; Zrev - primer reverse; Zcap - capture probe; Zamp - cDNA Target (PCR amplicon); **Dengue virus**: Damp - cDNA non complementary target. In supplementary material Scheme S-1 and S-2 the sequences of the NS5 protein coding regions in the genomes of zika and dengue viruses are shown, respectively.

Similarity primers were verified for six flaviviruses and the chikungunya virus using Basic Local Alignment Search Tool (BLAST) (Mcginnis and Madden, 2004), as shown in Table S-3. The observed similarity is considered a continuous sequence of equal bases, and the results presented in Table S-2 indicate a low similarity (≤ 11 bp) of the primers drawn (23 bp) in this study with genomes belonging to the same genre. Thus, based on the complementarity of the sequences, the identification of the zika and dengue virus by the analysis of the predicted PCR amplicon is specific, and, as a consequence, the capture probes can be used to differentiate these two diseases.

3.3. Electrochemical experiments in the gold-PET label-free biosensor

We first evaluated the biosensor optimization parameters, including electrode sensitivity experiments, such as pH (Fig. S-5), concentration (Fig. S-6), immobilization time (Fig. S-7), and immobilization temperature (Fig. S-8) of the capture probes, as presented in the Supplementary Materials section. The Nyquist diagram shows two important regions for the reactions on the surface of the solid electrode: The

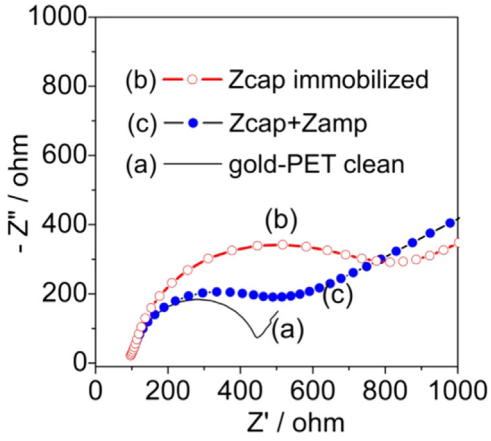

Fig. 2. Nyquist diagram representing the impedance behavior during the three stages of construction of the gold-PET biosensor: (a) clean electrode, solid black line; (b) immobilization of the capture sequence (Zcap), open circles (○) and (c) hybridization with Zamp, full blue circles (●). Immobilization of 0.40 µM of Zcap for 6 h at 45 °C and Zamp concentrations of 130 nM.

semicircle obtained by high frequency modulation describes the electron transfer processes, while the low frequency linear region contains information about the mass transport of the redox species at the electrolyte-electrode interface. The Randles model is best suited for modeling DNA biosensors when the Nyquist plots in the EIS have unique semicircles. Rct was used as the main parameter of investigation in the EIS technique, which was used to evaluate cleaning, capture sequence immobilization (Zcap), and complementary (Zamp)/non-complementary (Damp) sequence hybridizations.

In this study, the Nyquist diagram of the three steps in the gold-PET biosensor functionalized included the cleansing of the electrode, immobilization of the capture sequence (Zcap), and hybridization of the Zcap and complementary sequence (Zamp) for the zika virus, as shown in Fig. 2.

The curve corresponding to the electrode without any functionalization (gold-PET) was drawn in a continuous black line (Fig. 2), the immobilization step was represented by open circles, and hybridization by full circles. In these results, the clean gold-PET electrode presented Rct = (367 ± 15) Ω. After the immobilization of 0.40 µM of the capture sequence (Zcap), the load transfer resistance had an increase of (Rct = 970 ± 28) Ω, and after the hybridization with 130 nM of the complementary sequence (Zamp), there was a decrease in (Rct = 590 ± 22) Ω. However, it was getting larger than the initial impedance of the clean electrode. The resistance of the electrolyte was (99 ± 4) Ω, and the behavior of Rct was the same for the other concentrations of the complementary sequences studied here, which were presented in the selectivity assay in Fig. 4.

The behavior for the decrease of charge transfer resistance after hybridization is attributed to the new conformation of the secondary structure of the double-tape. Hant et al. investigated the distinct dynamics for the flexible single-stranded and stiff double-stranded DNA tethered to gold surfaces in electrolyte solution. Studies using time-resolved fluorescence measurements and hydrodynamic simulations showed that upper segments of the flexible ssDNA can dangle above its lower part, leading to significant coiling of the molecule. As a result, the average distance of the ssDNA's top end to the surface is reduced compared to dsDNA. For that reason, rigid dsDNA can be aligned more efficiently by repulsive electrode potentials than flexible ssDNA (Rant et al., 2006, 2004).

Gebala and Schuhmann (2010) investigated the conformation changes in the DNA sequence due to the polarization of the electrode interface during impedance measurements. Typically the EIS for DNA detection is measured in the presence of a negatively charged redox $[Fe(CN)_6]^{3-/4-}$ pair. The transfer rate of the redox marker, which will

determine the Rct value, is not only influenced by the accumulation of additional negative charges, but also by the physical blockade of the electrode surface, caused by ssDNA folding. This folding occurs due to the electrostatic attraction between the positively polarized surface and the negatively charged phosphate groups. The action of the electric field imposed during the EIS measurements may attract regions of the negatively charged capture ssDNA sequences (Zcap) to the surface of the electrode. After hybridization, the newly formed DNA double strands acquire greater rigidity to the folding caused by the electrostatic attraction, and, depending on the fraction of the surface released after hybridization, even a decrease of Rct can be observed.

Recently, Elshafey and coworkers explored the decreasing behavior of the Rct in an impedimetric DNA biosensor for detection of anthoxin (ATX), a neurotoxin found in cyanobacteria, to alter the conformation of the sequence (Elshafey et al., 2015). In this case, ATX associates with the free sequence, inducing a globular packaging at the free end which, as a consequence, opens sites for charge transfer. The effect is then used to quantify the concentration of ATX in the sample. The Elshafey study presents the results based on electrochemical measurements of CV, EIS, and DPV.

It is worth mentioning that numerous studies can be found on DNA biosensors that report the progressive increase of Rct in the two stages including immobilization and hybridization. Particularly, when the target sequence contains functionalization (eg., label), the blocking effect on the transfer of charges on the surface prevails over the effects of the conformation of the DNA secondary structure. In this study, capture sequences immobilization on biosensor was performed without the use of molecular intercalators such as mercaptohexanol (MCH). This strategy aimed to simplify the steps of biosensor construction and has already been presented in the literature as the biosensor proposed by Carpini et al. (2004), utilizing a thiol-DNA SAMs in the presence and absence of the MCH intercalator. Carpini showed mean differences of 6 µA less, compared with the measurements in the thiol-DNA + MCH biosensor. This work also shows that the simpler configuration yields reliable results for concentrations above 10 M in the detection of the target sequence. In the same work, a calibration curve for concentrations between 0.12 and 1230 µM shows that the biosensor enters saturation at 200 nM of the target sequence. This suggests an analytical window of concentration between 10 and 200 nM for this type of SAMs is only with thiol-DNA, without MCH.

Voltammetric measurements in gold-PET biosensor confirm the behavior observed in the EIS, i.e., the decrease of charge transfer resistance after hybridization (Fig. 3). Immobilization of 0.40 µM of Zcap for 6 h at 45 °C and Zamp concentrations of 130 nM, the same EIS. The initial peak current of 58.7 µA on the clean electrode decreased to 11.8 µA after Zcap immobilization. After hybridization with Zamp at

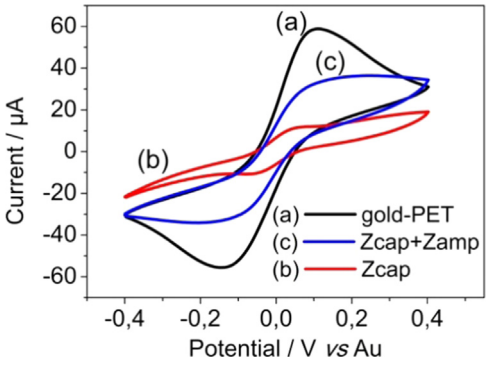

Fig. 3. Cyclic voltammetry of the construction steps of the gold-PET biosensor in the drop system: (a) clean electrode, black line curve; (b) immobilization of the capture sequence (Zcap), red curve and (c) hybridization, blue curve. Immobilization of 0.40 µM of Zcap for 6 h at 45 °C and Zamp concentrations of 130 nM.

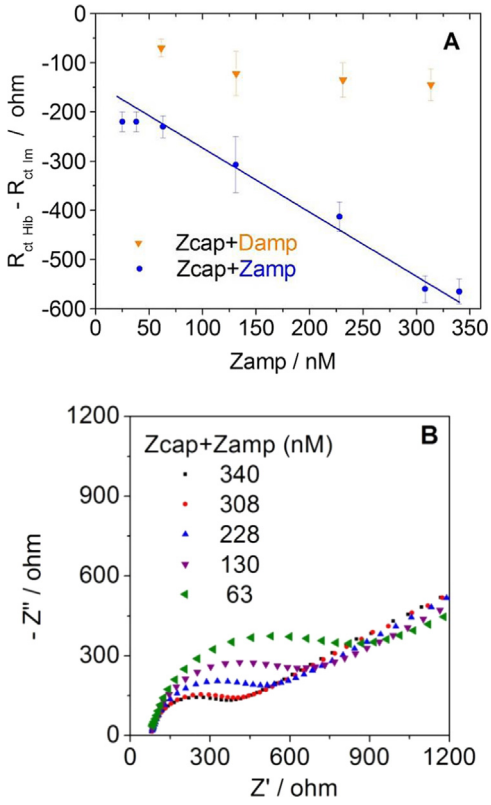

Fig. 4. (A) Analytical curve of charge transfer resistance (ΔRct = Rct Hib - Rct Im): (A) Immobilization of 0.40 µM of the capture sequence (Zcap) for 5 h at 45 °C. Hybridization with Zamp, blue circle (●) at concentrations of 25, 38, 63, 130, 228, 308 and 340 nM and negative control with Damp, orange triangle (▼) at the concentration of 63, 130, 228 and 308 nM. (B) Nyquist plots after Zcap + Zamp hybridization at five concentrations included in the linear region. EIS performed in a drop of 60 µL, three separate electrodes for each concentration (n = 3).

the concentration of 130 nM, it rose again to 36.8 µA. Another frequently used technique for the characterization of DNA biosensors is differential pulse voltammetry (DPV). Fig. S-9 shows DPV results.

In the selectivity assays, Fig. 4A, the biosensor functionalized with Zcap capture sequences was placed to hybridize with complementary sequences (Zamp) at concentrations of 25, 38, 63, 130, 228, 308 and 340 nM, indicated by (ΔRct = Rct Hib – Rct Im), were Rct Hib: value hybridized sequences and Rct Im: value Zcap immobilized. In the calibration curve, Fig. 4A, the concentration of 63, 130, 228 and 308 nM makes the distinction between ΔRct values in complementary hybridizations (Zcap + Zamp) and non-complementary (Zcap-Damp). Fig. 4B shows the Nyquist plots after the complementary hybridization at the concentrations included in the linear region of the calibration curve, using three distinct electrodes for error bar.

The Nyquist plots comparing the Zcap hybridizations with Zamp and Damp, both at the critical concentration of 130 nM, are shown in Fig. 5. In the Nyquist plot, the blank circle curve represents the Zcap immobilized electrode at Rct Im = (970 ± 28) Ω which, after hybridization with Zamp, showed the decrease of the load transfer resistance of Rct Hib (490 ± 22) Ω, which represents a difference for the immobilized electrode of ΔRct = (–480 ± 50) Ω. Hybridization with Damp Rct = (860 ± 17) Ω, at the same concentration of 130 nM, resulted in a ΔRct = (–110 ± 45) Ω. The resistance of the electrolyte was (120 ± 5) Ω. This decrease in non-complementary hybridization can be attributed to the Damp sequences that remained electrostatically bound to the electrode even after washing. However, the difference of Rct for the complementary and non- complementary (370 ± 05) Ω is sufficient to guarantee the biosensor's selectivity for detecting

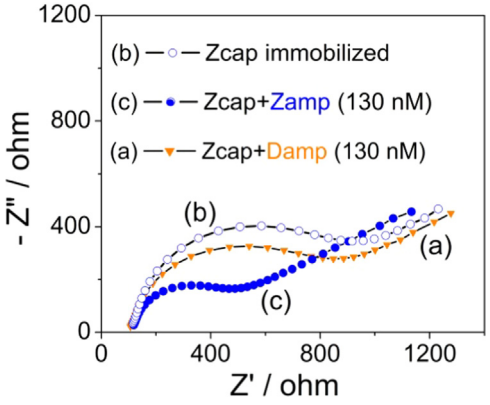

Fig. 5. Comparative Nyquist plot for the complementary and non- complementary hybridizations: (b) Zcap capture sequences immobilized on the electrode, blank circle (○); (c) Zcap hybridized with complementary sequence Zamp, blue circle, (●) in the concentration of 130 nM and (a) Zcap hybridized with a non-complementary sequence Damp, orange triangle (▼), in the concentration of 130 nM.

sequences that identify zika, in the linear window of calibration curve.

In the gold-PET biosensor, the detection limit was calculated using the electrode blank curves from seven electrodes, with a SD of 9.86 and a slope of the best fit line where b = -1.18 ± 0.08 and R^2 = 0.986 (Fig. 4), resulting in the limit of detection LOD_{IUPAC} = (25.0 ± 1.7) nM. The reproducibility of the DNA biosensor on the gold-PET electrode was estimated at the concentration of the target sequence of 130 nM, data from the calibration curve of Fig. 4. The relative deviation between independent electrodes (n = 5) was 17% and for measurements on the same electrode 5% (n = 5). These results indicated that the reproducibility of the biosensors allows for differentiation between the complementary sequence (Zamp) and the non-complementary sequence (Damp).

Table 1 compares two groups of biosensors developed for molecular analysis. The first group consists of three colorimetric systems reported in the last two years, and the second group includes electrochemical detection methods, including this work.

In Table 1, the methods of molecular analysis are compared. The first three methods use colorimetry as a detection method associated with the isothermal techniques of RNA amplification, while the last three present electroanalytical methods for the analysis of the hybridization events. To show a comparison between other electrochemical biosensors, the works of Zhang (2010) and Zheng (2013) that analyzed the acquired immunodeficiency virus (HIV) were cited (Zhang et al., 2010; Zheng et al., 2013). To the best of our knowledge, there are no reported literature on an electrochemical biosensor for the molecular analysis of the zika virus.

The label-free electrochemical biosensor for the molecular analysis of the zika virus may be an alternative to the colorimetric biosensors. The first advantage presented by this system is the use of label-free detection, which simplifies the sample preparation process. From a sample previously amplified by RT-PCR or isothermal techniques, the hybridization event indicates the positive or negative detection of the zika virus through one of the electrochemical techniques such as EIS, CV, or DPV. The biosensor developed in this study has a detection range between 25 nM and 340 nM, surpassing the other two electrochemical biosensors presented in Table 1. The sample volume used (60 µL) was the smallest among the six devices listed in Table 1, revealing a relevant feature for point-of-care use. The assay time is very similar to that of the colorimetric biosensors.

In summary, the DNA biosensor on the gold-PET electrode is suitable for reliable detection of the target sequences of interest at concentrations above 54 nM. The biosensor showed sufficient reproducibility to identify the sequence of interest with confidence, and is promising for use as a molecular diagnostic devices for infectious diseases such as zika and dengue.

4. Conclusion

This study reports the construction of a label-free electrochemical biosensor for the detection of zika virus synthetic DNA sequences. The gold-PET label-free zika biosensor showed relevant properties since the analysis using a one sample drop and the detection was obtained without the need for DNA tagging or the use of reagents. The disposable electrodes are cost-effective, which allows for large-scale application, and exhibited selectivity toward Zika virus sequences, with a detection limit of 25.0 nM, using a calibration curve that evaluated the concentration range of 25–340 nM. The biosensors exhibited good reproducibility and allowed the differentiation between the complementary sequence of zika virus and the non-complementary sequence for dengue virus. The small sample volume used, as well as the time required for analyses - ca. ninety minutes - represent relevant features for point-of-care applications. Our results suggests that the biosensors developed are promising for integration with PCR technology for the molecular analysis of virus, such as zika and dengue. As the biosensor should act after the sequence amplification process, it will also be useful upon association with both the RT-PCR technique and isothermal techniques, such as NASBA and RT-Lamp. Although the molecular analysis was performed in synthetic DNA, it is nonetheless necessary to continue research into gold-PET label-free zika biosensor in order to further develop their protocols for molecular analysis with real samples of zika, dengue and others virus.

Credit authorship taxonomy statement

Henrique Antonio Mendonça Faria: Conceptualization, Formal analysis, Methodology, Software, Writing - original draft. **Valtencir Zucolotto**: Conceptualization, Formal analysis, Funding acquisition, Project administration, Supervision, Writing - review & editing

Table 1
DNA and zika RNA biosensors.

Assay technique	Detection mode	Disease	Target	Range of detection	Limit of detection	Sample volume	Assay time	Ref.
NASBA-CRISPR	Colorimetry	Zika virus	RNA	3–30 fM	1 fM	300 µL	1 h	Pardee (2016)
RT-Lamp	Colorimetry	Zika virus	RNA (E protein)	50–5 × 10^4 PFU/mL	50–100 × 10^4 PFU/mL	65 µL	40 min	Song (2017)
RT-Lamp	Colorimetry	Zika virus	RNA (NS1 protein)	–	1.6 × 10^5 PFU/mL	Micro-fluidic	1 h	Ganguli (2017)
EIS SWV	Electrochemical Metilene blue	HIV	DNA	1–250 nM	1 × 10^{-1} nM	100 µL	1 h	Zhang (2010)
EIS	Electrochemical Label-free	HIV	DNA	0.1–40 nM	4 × 10^{-2} nM	Electro-chemical cell	4 h	Zheng (2013)
EIS CV DPV	Electrochemical Label-free	Zika virus	RNA (NS5 protein)	54–340 nM	25 nM	60 µL	1.5 h	This work (2019)

Acknowledgments

The authors gratefully acknowledge LNNANO, Campinas-Brazil, from support AFM measurement and financial support from CNPq, Brazil (grant number 440496/2016-0) and CAPES, Brazil (grant number 88881.130763/2016-01) and (grant number 2013–57062390615).

Competing interests statement

There are no competing interests to declare.

Appendix A. Supporting information

Supplementary data associated with this article can be found in the online version at doi:10.1016/j.bios.2019.02.018.

References

Bhatt, S., Gething, P.W., Brady, O.J., Messina, J.P., Farlow, A.W., Moyes, C.L., Drake, J.M., Brownstein, J.S., Hoen, A.G., Sankoh, O., Myers, M.F., George, D.B., Jaenisch, T., Wint, G.R., William, S., Cameron, P., Scott, T.W., Farrar, J.J., Hay, S.I., 2013. Nature 496, 504–507.
Carpini, G., Lucarelli, F., Marrazza, G., Mascini, M., 2004. Biosens. Bioelectron. 20, 167–175.
Chang, B.Y., Park, S.M., 2010. Annu. Rev. Anal. Chem. 3, 207–228.
Chen, C.P., Ganguly, A., Wang, C., Hsu, C.W., Chattopadhyay, S., Hsu, Y.K., Chang, Y.C., Chen, K.H., Chen, L.C., 2009. Anal. Chem. 81, 36–42.
Compton, J., 1991. Nature 350 (6313), 91–92.
Elshafey, R., Siaj, M., Zourob, M., 2015. Biosens. Bioelectron. 68, 295–302.
Fauci, A.S., Morens, D.M., 2016. N. Engl. J. Med. 374, 601–604.
Ganguli, A., Ornob, A., Yu, H., Damhorst, G., Chen, W., Sun, F., Bhuiya, A., Cunningham, B., Bashir, R., 2017. Biomed. Microdev. 19, 73.
Gebala, M., Schuhmann, W., 2010. Chemphyschem 11, 2887–2895.
Gebala, M., Schuhmann, W., 2012. Phys. Chem. Chem. Phys. 14, 14933–14942.
Golan, Y., Margulis, L., Rubinstein, I., 1992. Surf. Sci. 264 (3), 312–325.
Gooding, J.J., Darwish, N., 2012. Chem. Rec. 12, 92–105.
Haug, C.J., Kieny, M.P., Murgue, B., 2016. N. Engl. J. Med. 374, 1801–1803.
Hoogvliet, J.C., Dijksma, M., Kamp, B., van Bennekom, W.P., 2000. Anal. Chem. 72, 2016–2021.
Ingebrandt, S., Han, Y., Nakamura, F., Poghossian, A., Schoening, M.J., Offenhaeusser, A., 2007. Biosens. Bioelectron. 22, 2834–2840.
Janegitz, B.C., Cancino, J., Zucolotto, V., 2014. J. Nanosci. Nanotechnol. 14, 378–389.
Keighley, S.D., Li, P., Estrela, P., Mighorato, P., 2008. Biosens. Bioelectron. 23, 1291–1297.
Labuda, J., Brett, A.M.O., Evtugyn, G., Fojta, M., Mascini, M., Ozsoz, M., Palchetti, I., Palecek, E., Wang, J., 2010. Pure Appl. Chem. 82, 1161–1186.
Li, C.Z., Liu, Y.L., Luong, J.H.T., 2005. Anal. Chem. 77, 478–485.
Lisdat, F., Schaefer, D., 2008. Anal. Bioanal. Chem. 391, 1555–1567.
Mcginnis, S., Madden, T.L., 2004. Nucleic Acids Res. 32, W20–W25.
Musso, D., Roche, C., Nhan, T.X., Robin, E., Teissier, A., Cao-Lormeau, V., 2015. J. Clin. Virol. 68, 53–55.
Notomi, T., Okayama, H., Masubuchi, H., Yonekawa, T., Watanabe, K., Amino, N., Hase, T., 2000. Nucleic Acids Res. 28 (12), E63.
Oliveira, O.N., Iost, R.M., Siqueira, J.R., Crespilho, F.N., Caseli, L., 2014. ACS Appl. Mater. Interfaces 6 (17), 14745–14766.
Ozsoz, M., 2012. **Electrochemical DNA Biosensors**. Pan Stanford Publishing, Singapure.
Papadopoulou, E., Goodchild, S.A., Cleary, D.W., Weller, S.A., Gale, N., Stubberfield, M.R., Brown, T., Bartlett, P.N., 2015. Anal. Chem. 87, 1605–1611.
Pardee, K., Green, A.A., Takahashi, M.K., Braff, D., Lambert, G., Lee, J.W., Ferrante, T., Ma, D., Donghia, N., Fan, M., Daringer, N.M., Bosch, I., Dudley, D.M., O'Connor, D.H., Gehrke, L., Collins, J.J., 2016. Cell 165, 1255.
Park, J.Y., Kwon, S.H., Park, J.W., Park, S.M., 2008. Anal. Chim. Acta 619, 37–42.
Patolsky, F., Lichtenstein, A., Willner, I., 2001. Nat. Biotechnol. 19, 253–257.
Petersen, L.R., Jamieson, D.J., Powers, A.M., Honein, M.A., 2016. N. Engl. J. Med. 374, 1552–1553.
Rant, U., Arinaga, K., Tornow, M., Kim, Y.W., Netz, R.R., Fujita, S., Yokoyama, N., Abstreiter, G., 2006. Biophys. J. 90, 3666–3671.
Rant, U., Arinaga, K., Fujita, S., Yokoyama, N., Abstreiter, G., Tornow, M., 2004. Langmuir 20, 10086.
Singh, R.K., Dhama, K., Karthik, K., Tiwari, R., Khandia, R., Munjal, A., Iqbal, H.M.N., Malik, Y.S., Marí, R.B., 2018. Front. Microbiol. 8, 2677.
Song, J., Liu, C., Mauk, M.G., Rankin, S.C., Lok, J.B., Greenberg, R.M., Bau, H.H., 2017. Clin. Chem. 63, 714–722.
Thompson, J.D., Gibson, T.J., Plewniak, F., Jeanmougin, F., Higgins, D.G., 1997. Nucleic Acids Res. 25, 4876–4882.
Watterson, J., Piunno, P.A.E., Krull, U.J., 2002. Anal. Chim. Acta 469, 115–127.
Witte, C., Lisdat, F., 2011. Electroanalysis 23, 339–346.
Yan, Y.R., Ding, S.J., Zhao, D., Yuan, R., Zhang, Y.H., Cheng, W., 2016. Sci. Rep. 6, 18810.
Yang, K.-H., Narayan, R.J., 2017. MRS Commun. 7, 121–130.
Zhang, D., Peng, Y., Qi, H., Gao, Q., Zhang, C., 2010. Biosens. Bioelectron. 25, 1088–1094.
Zheng, H., Ma, X., Chen, L., Lin, Z., Guo, L., Qiu, B., Chen, G., 2013. Anal. Methods 5, 5005–5009.